Enhancement of average thermoelectric figure of merit by increasing the grain-size of $Mg_{3.2}Sb_{1.5}Bi_{0.49}Te_{0.01}$

Tsutomu Kanno, Hiromasa Tamaki, Hiroki K. Sato, Stephen Dongmin Kang, Saneyuki Ohno, Kazuki Imasato, Jimmy Jiahong Kuo, G. Jeffrey Snyder, and Yuzuru Miyazaki

Citation: Appl. Phys. Lett. **112**, 033903 (2018);
View online: https://doi.org/10.1063/1.5016488
View Table of Contents: http://aip.scitation.org/toc/apl/112/3
Published by the American Institute of Physics

Enhancement of average thermoelectric figure of merit by increasing the grain-size of $Mg_{3.2}Sb_{1.5}Bi_{0.49}Te_{0.01}$

Tsutomu Kanno,[1,a)] Hiromasa Tamaki,[1] Hiroki K. Sato,[1] Stephen Dongmin Kang,[2,3] Saneyuki Ohno,[2,3,4] Kazuki Imasato,[2] Jimmy Jiahong Kuo,[2] G. Jeffrey Snyder,[2] and Yuzuru Miyazaki[5]

[1]*Advanced Research Division, Panasonic Corporation, Seika, Kyoto 619-0237, Japan*
[2]*Department of Materials Science and Engineering, Northwestern University, Evanston, Illinois 60208, USA*
[3]*Department of Applied Physics and Materials Science, California Institute of Technology, Pasadena, California 91125, USA*
[4]*Institute of Physical Chemistry, Justus-Liebig-University Giessen, Heinrich-Buff-Ring 17, 35392 Giessen, Germany*
[5]*Department of Applied Physics, Tohoku University, Sendai, Miyagi 980-8579, Japan*

(Received 20 November 2017; accepted 27 December 2017; published online 17 January 2018)

Zintl compound n-type $Mg_3(Sb,Bi)_2$ was recently found to exhibit excellent thermoelectric figure of merit zT (~1.5 at around 700 K). To improve the thermoelectric performance in the whole temperature range of operation from room temperature to 720 K, we investigated how the grain size of sintered samples influences electronic and thermal transport. By increasing the average grain size from 1.0 μm to 7.8 μm, the Hall mobility below 500 K was significantly improved, possibly due to suppression of grain boundary scattering. We also confirmed that the thermal conductivity did not change by increasing the grain size. Consequently, the sample with larger grains exhibited enhanced average zT. The calculated efficiency of thermoelectric power generation reaches 14.5% ($\Delta T = 420$ K), which is quite high for a polycrystalline pristine material. *Published by AIP Publishing.* https://doi.org/10.1063/1.5016488

Thermoelectric power generation is a solid-state, scalable, and direct energy conversion process from heat into electricity.[1,2] The performance of thermoelectric materials is evaluated using the material figure of merit $zT = S^2T/(\rho\kappa)$, where S is the Seebeck coefficient, ρ is the electrical resistivity, κ is the thermal conductivity of thermoelectric materials, and T is the absolute temperature. In thermoelectric power generation, the temperature difference applied across a thermoelectric material could reach several hundred K, depending on heat sources. A problem is that zT and its constituent parameters, S, ρ, and κ, are generally a strong function of temperature. Thus, it is challenging to achieve a high average zT, which is crucial to realize high conversion efficiency. Recent progress in understanding the relationship between materials chemistry and thermoelectric transport has unveiled high average zT by modifying the composition and texture of existing materials. Examples of such materials include hole-doped single-crystalline SnSe[3] and PbS-alloyed PbTe with a phase-separated nanostructure.[4]

Recently, Tamaki *et al.* found that the n-type Zintl compound Mg_3Sb_2 with a modified nominal composition, $Mg_{3.2}Sb_{1.5}Bi_{0.49}Te_{0.01}$, has excellent $zT \sim 1.5$ at 716 K.[5] Since the first report, at least two groups have not only reproduced the result but also reported improved average zT either by compositional modification or by different sintering temperatures.[6–10] Te is an n-type dopant; Se has also been investigated as a donor.[9,11] The appropriate nominal composition to optimize the thermoelectric properties depends on preparation techniques, but generally, Mg excess in the nominal composition is required to mitigate Mg vacancies and stabilize the n-type character of this material. Considering charge balance and defect formation energies, the actual composition of the main phase is close to $Mg_3Sb_{1.5}Bi_{0.49}Te_{0.01}$.[12] Shuai *et al.*[6] reported suppression of electron scattering below 500 K in Nb-incorporated $Mg_{3.2-x}Nb_xSb_{1.5}Bi_{0.49}Te_{0.01}$. Zhang *et al.*[7] reported a similar improvement in the Hall mobility in $Mg_3Sb_{1.5-x}Bi_{0.5-0.5x}Te_x$ samples, whose composition is almost the same as that in Ref. 5, but the sintering temperature was significantly higher (1123 K) compared with Refs. 5 and 6. (873 K). Comparison of these results suggests that the microstructure of Mg_3Sb_2 samples has a strong influence on the Hall mobility, but the details remained unknown.

Here, we investigated the relationship between the microstructure and thermoelectric properties in $Mg_{3.2}Sb_{1.5}Bi_{0.49}Te_{0.01}$. We found that, by increasing the grain size, electron scattering was significantly suppressed while the thermal conductivity was kept unchanged. Enhanced average zT was observed in the sample with the average grain size of 7.8 μm, and the calculated efficiency at the temperature difference of 420 K reaches 14.5%.

We prepared samples with a nominal composition of $Mg_{3.2}Sb_{1.5}Bi_{0.49}Te_{0.01}$, which is the same as that of Ref. 5, by mechanical alloying and spark plasma sintering. Elemental powders of Mg, Sb, Bi, and Te were used as starting materials. In the mechanical alloying process, elemental powders were loaded to a stainless-steel jar in an Ar-filled glove box and subjected to planetary ball-milling. Here, a multistep milling process was adapted by using stearic acid as a milling agent. The details of the process can be found elsewhere.[5] Next, the mechanically alloyed powder (~3 g) was filled in a graphite die (φ 10 mm) in an Ar-filled glove

a)E-mail: kanno.tsutomu@jp.panasonic.com

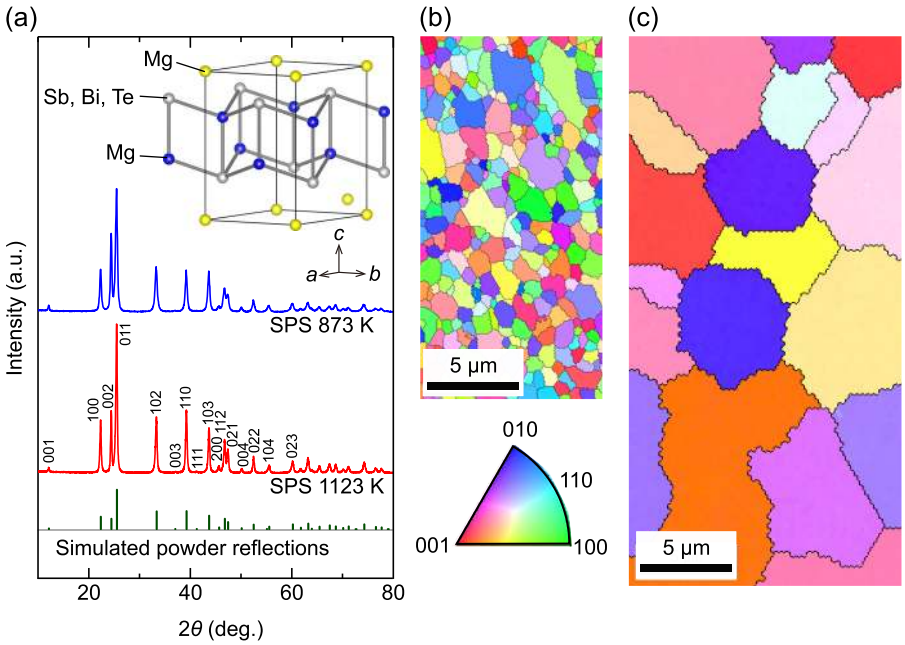

FIG. 1. (a) XRD patterns of the polished surface of sintered $Mg_{3.2}Sb_{1.5}Bi_{0.49}Te_{0.01}$ samples obtained using Cu-Kα radiation (Rigaku RINT-TTR III; Japan). Inset: crystal structure of $Mg_3(Sb,Bi,Te)_2$. (b) EBSD crystal-orientation maps of the sample sintered at 873 K (average grain size: 1.0 μm) and (c) 1123 K (average grain size: 7.8 μm). Map colors are assigned using the inverse pole figure (IPF) color scheme shown in the legend under (b). Grain boundaries were drawn where the misorientation angle between grains is more than 15°. The grain size was averaged over a 20 μm × 10 μm area [Fig. 1(b)] for the sample sintered at 873 K and a 180 μm × 60 μm area (see supplementary material S2) for the sample sintered at 1123 K. EBSD measurement was performed using an EBSD detector (EDAX; USA) equipped with a scanning electron microscope (Zeiss Supra 55VP; Germany).

box and loaded into a spark plasma sintering (SPS) chamber. SPS was performed in an Ar atmosphere of approximately 0.05 MPa. During the SPS process, a uniaxial pressure of 50 MPa was applied. To compare the thermoelectric properties of samples with different grain sizes, we prepare two kinds of samples with different SPS temperatures, 873 K and 1123 K. The sintered pellets had the shape of approximately 10 mm in diameter and 9 mm in height. The relative density was within the range between 92% and 96%. We cut the pellets into a rectangular shape (approximately 2 mm × 2 mm × 8 mm) for the measurement of the Seebeck coefficient and the electric resistivity and into a disk shape (approximately φ10 mm × 1 mm) for the thermal conductivity and the Hall measurement.

Figure 1(a) shows X-ray diffraction (XRD) patterns of the polished surface of sintered $Mg_{3.2}Sb_{1.5}Bi_{0.49}Te_{0.01}$ samples. Comparing the measured diffraction intensities with those of the simulated powder reflections (see supplementary material S1 for the crystal structure refinement), one can notice that the samples have no preferential crystalline orientation. Indeed, we confirmed no noticeable difference in thermoelectric properties between measurements in different directions with respect to the pressing direction during SPS. The XRD pattern for the sample sintered at 1123 K has relatively sharp peak profiles, which imply that there exists a difference in sample crystallinity. Figures 1(b) and 1(c) show crystal-orientation maps obtained by the electron backscattering diffraction (EBSD) technique.[13] A large difference in the grain size was observed: the average grain size was 1.0 μm and 7.8 μm for the samples sintered at 873 K and 1123 K, respectively (supplementary material S2). Using energy-dispersive X-ray spectroscopy (EDS) and inductively coupled plasma atomic emission spectroscopy (ICP-AES), we observed that elemental compositions of both samples were almost the same as the nominal composition (supplementary material S3).

In contrast to the typical strategy to nanostructure thermoelectric materials to reduce thermal conductivity, the thermal conductivity shown in Fig. 2(a) did not increase after growing the grain size by a factor of 8 (from 1.0 μm to 7.8 μm). This result can be explained considering the accumulated lattice thermal conductivity (ALTC) as a function of the phonon mean-free-path [Fig. 2(b)] for Mg_3Sb_2 at 300 K calculated using Phono3py.[14] The limit of ALTC at an infinitely large phonon mean free path corresponds to the lattice thermal conductivity of a large single crystal. One can notice that ALTC is quite isotropic despite the layered crystal structure [see the inset of Fig. 1(a)] and saturates around 0.6 μm in the *ab* plane and 1.8 μm along the *c* axis. The similar thermal conductivities for the average grain size of 1.0 μm and 7.8 μm is reasonable because both are already near the saturated region of ALTC. In addition, one can conclude that the observed low thermal conductivity of $Mg_{3.2}Sb_{1.5}Bi_{0.49}Te_{0.01}$ is intrinsic and not due to boundary scattering of phonons. Similar behavior is also observed in thermoelectric compounds with low intrinsic lattice thermal conductivity, e.g., PbTe,[15] $Mg_2(Si,Sn)$,[16] and ZrCoSb,[17] whose ALTC as a function of mean free path saturates around 10^0–10^1 μm (at room temperature) such that the grain size in this range is

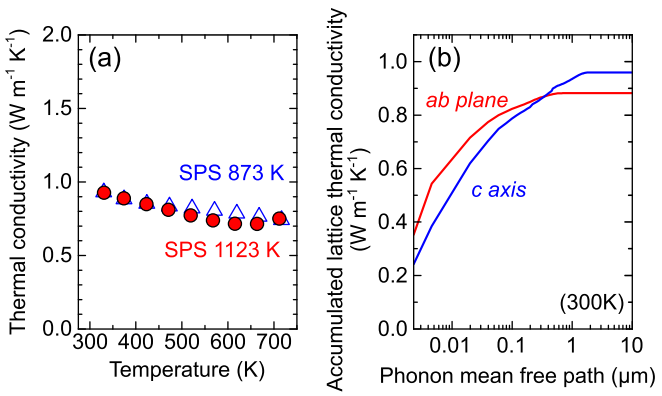

FIG. 2. (a) Thermal conductivity of $Mg_{3.2}Sb_{1.5}Bi_{0.49}Te_{0.01}$ sintered at 873 K and 1123 K. (b) Accumulated lattice thermal conductivity of Mg_3Sb_2 at room temperature as a function of phonon mean-free-path.

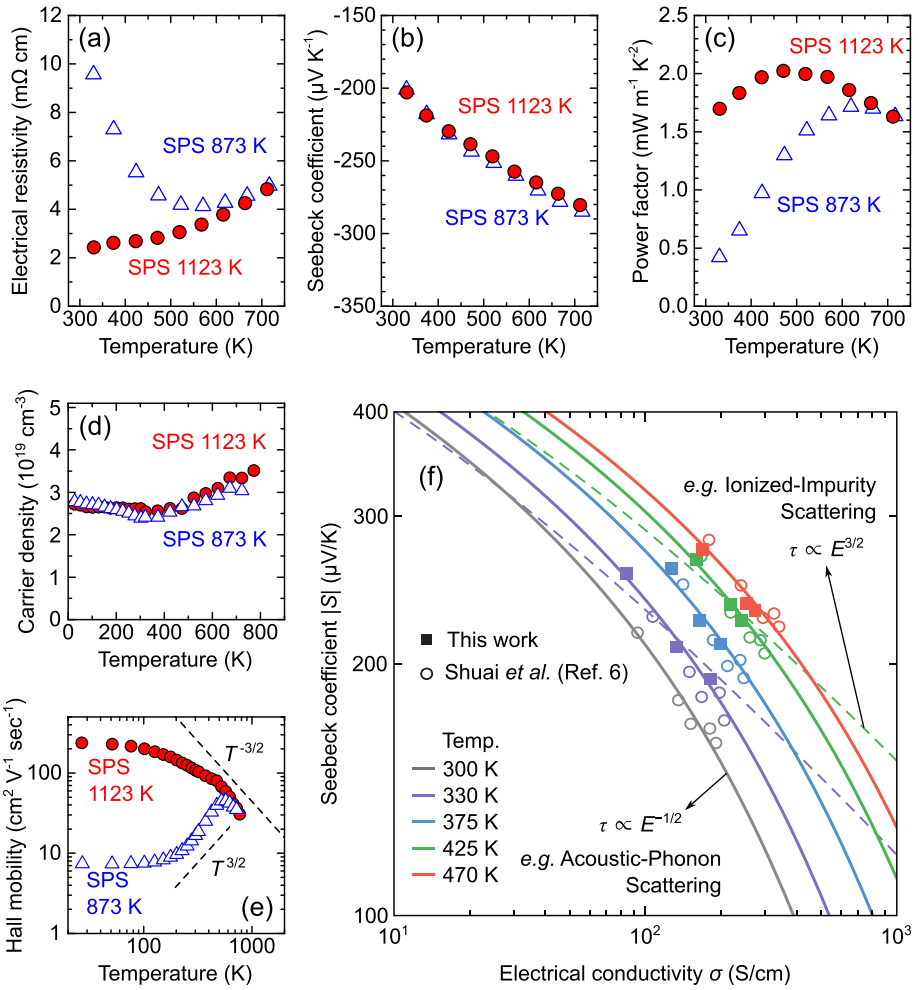

FIG. 3. (a) Electrical resistivity, (b) Seebeck coefficient, (c) power factor ($=S^2/\rho$), (d) carrier density, and (e) Hall mobility of $Mg_{3.2}Sb_{1.5}Bi_{0.49}Te_{0.01}$ sintered at 873 K and 1123 K. (f) Comparison of the experimentally found $\log|S| - \log\sigma$ relation with different energy dependent scattering models. At all temperatures between 300 and 470 K, better agreement with the curve shape of $\tau \propto E^{-1/2}$ (rather than $\tau \propto E^{3/2}$) is found, which is an energy dependency that is predicted by acoustic-phonon and point defect scattering models rather than ionized impurity scattering (see Table I). The open circle data points are from the literature where thermally activated conduction was attributed to ionized impurity scattering.[6] Solid square data points are from a group of samples in this work (with smaller grain size) that had similar low temperature resistivity.

large enough to utilize all the lattice thermal conductivity reduction possible from nanostructuring.

The large grain size has a positive impact on the electronic transport and the thermoelectric performance. The electrical resistivity of the sample sintered at 1123 K was significantly reduced and showed metallic behavior [Fig. 3(a)]. The Seebeck coefficient did not change significantly [Fig. 3(b)], and thus, we achieved considerable enhancement in the power factor especially below 500 K [Fig. 3(c)]. These results are reasonable if we assume that electron scattering of extrinsic origins, e.g., grain boundary scattering, was suppressed without changing the intrinsic material properties such as the electronic band structure and the carrier concentration.

To further investigate the electronic transport of $Mg_{3.2}Sb_{1.5}Bi_{0.49}Te_{0.01}$ samples sintered at different SPS temperatures, we performed Hall measurements using the van der Pauw technique. Figures 3(d) and 3(e) show the carrier density and the Hall mobility, respectively. We observe a similar carrier density of 2.5–3.5 $\times 10^{19}$ cm^{-3} for both samples. For the sample sintered at 1123 K, we observed a higher mobility (108 cm^2 V^{-1} s^{-1} at 300 K), which monotonically increases with decreasing temperature. Conversely, the mobility of the sample sintered at 873 K decreases at lower temperature due to strong electron scattering although it had the similar value at around 700 K. The temperature dependency at higher temperature may be explained well by the acoustic phonon scattering ($\sim T^{-3/2}$) with additional contribution from excited optical phonons. The increasing Hall mobility with respect to temperature (observed at $<$500 K) was previously attributed to ionized-impurity scattering.[5,6] However, we find that the temperature dependency below 500 K is more complex and cannot be explained by a single mechanism, e.g., ionized-impurity scattering ($\sim T^{3/2}$).

Investigation of the $\log|S| - \log\sigma$ relation (at each temperature) shown in Fig. 3(f) indicates that the energy dependency of the charge carrier scattering time is not well explained with a simple ionized impurity scattering model. The curve shape of the $\log|S| - \log\sigma$ plot is indicative of the energy exponent r of the carrier relaxation time τ

$$\tau(T,E) = \tau_0(T) \cdot \left(\frac{E}{k_B T}\right)^r.$$

Here, E is the free carrier energy of the charge carrier and τ_0 is a reference scattering time at $E = k_B T$. As an example, in the degenerate limit (low thermopower), $|S| \propto \sigma^{\frac{1}{r+1.5}}$ [see supplementary information in Ref. 18]. The ionized impurity scattering model predicts $r = 3/2$, whereas the acoustic-phonon scattering model predicts $r = -1/2$ (Table I); the

TABLE I. Parameters for various scattering models.[19]

Scattering mechanism	Scattering parameter (r)	$\tau_0(T)$
Point defects	$-1/2$	$\propto T^{-\frac{1}{2}}$
Acoustic phonons	$-1/2$	$\propto T^{-\frac{3}{2}}$
Ionized impurities	3/2	$\propto T^{\frac{3}{2}}$

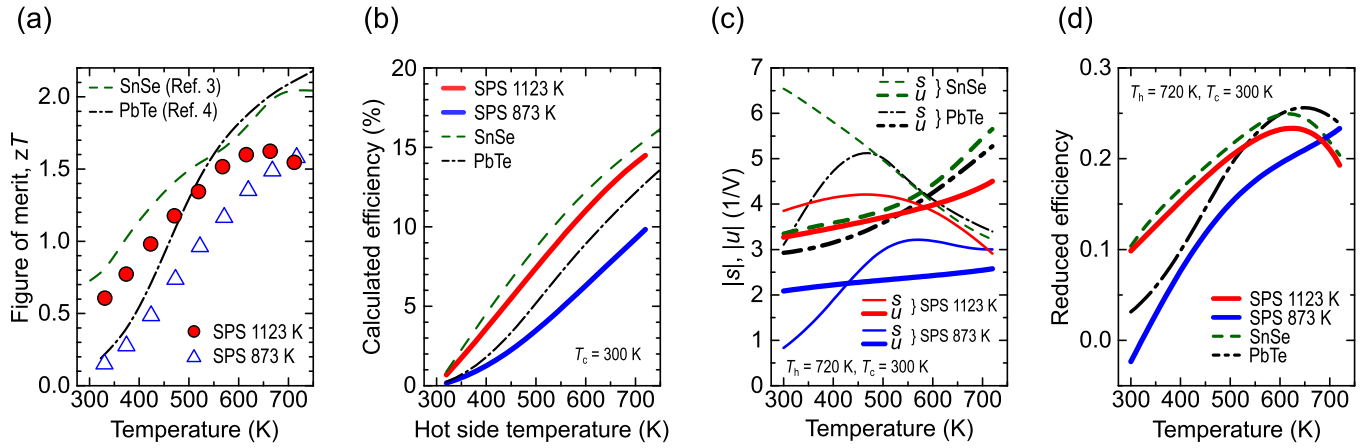

FIG. 4. (a) Figure of merit zT, (b) calculated conversion efficiency, (c) absolute values of compatibility factor $|s|$ and relative current density $|u|$, and (d) reduced efficiency η_r of $Mg_{3.2}Sb_{1.5}Bi_{0.49}Te_{0.01}$ sintered at 873 K and 1123 K. Properties of a hole-doped SnSe single crystal along the b axis[3] and PbS-alloyed PbTe with the phase separated nanostructure[4] were plotted for comparison. In (b)–(d), the cold side temperature T_c was fixed to be 300 K. For (c) and (d), the hot side temperature T_h was fixed to be 720 K. The efficiency, s, u, and η_r were calculated using the spreadsheet calculator reported in Ref. 22.

$\log|S| - \log\sigma$ curves of each model are shown in Fig. 3(f) to have a different slope in the low $|S|$ regime due to different exponents r. Comparison of experimental data to the scattering model curves in Fig. 3(f) shows that the energy dependency of scattering time better resembles acoustic phonon scattering than ionized impurity scattering at all temperatures from 300 to 470 K.

The fact that the energy dependency (similar to acoustic phonon scattering) and temperature dependency (thermally activated such as ionized impurity scattering) do not provide a consistent description indicates that a model different than those listed in Table I is required to adequately describe the transport of $Mg_{3.2}Sb_{1.5}Bi_{0.49}Te_{0.01}$. The grain size dependency found in our current work suggests that grain boundary effects must be addressed for a good model description. Details of this grain boundary transport model are published elsewhere.[20]

Consequently, the thermoelectric figure of merit zT was significantly improved in the whole measured temperature range [Fig. 4(a)]. For comparison, zT of state-of-the-art thermoelectric materials, hole-doped SnSe single crystal along the b axis,[3] and PbS-alloyed PbTe with the phase separated nanostructure[4] were also plotted. To examine how the present improvement of thermoelectric properties affects the energy conversion performance, we calculated the conversion efficiency. The efficiency of a thermoelectric material with temperature-dependent properties under a given operating condition is precisely calculated by considering thermoelectric compatibility.[21,22] Here, a material is regarded as a series connection of infinitesimally sliced elements, each of which has different local temperatures and thermoelectric properties. Optimization of the efficiency is done by adjusting the relative current density $u = J/(\kappa\nabla T)$, where J is the electric current density. The reduced efficiency $\eta_r = u(S - u\rho\kappa)/(uS + 1/T)$, which is a local parameter in a material subjected to a temperature difference, determines the overall efficiency. η_r is maximized when $u = s = \left(\sqrt{1+zT} - 1\right)/(ST)$, where s is the compatibility factor. In general, however, u inevitably deviates from s because u must also satisfy the heat flow equation, $\nabla(\kappa\nabla T) = -T\frac{dS}{dT}J\nabla T - \rho J^2$, at any point of a material. Therefore, to enhance the efficiency, it is important to have both high average zT and small deviation of u from s in the whole temperature range of operation.

We confirmed a large enhancement in the calculated conversion efficiency [Fig. 4(b)] due to the improvement of average zT. The maximum efficiency of $Mg_{3.2}Sb_{1.5}Bi_{0.49}Te_{0.01}$ sintered at 1123 K was 14.5% (cf. 9.8% for the sample sintered at 873 K) with the temperature difference of 420 K ($T_h = 720$ K and $T_c = 300$ K). The efficiency is almost the same as hole-doped single-crystalline SnSe[3] (15.4%) and PbS-alloyed PbTe with the phase-separated nanostructure[4] (12.7%), despite the large difference in the peak zT. The high efficiency can be explained by the smaller deviation of the relative current density u from the compatibility factor s compared with that of SnSe and PbTe [Fig. 4(c)]. As is also shown in the reduced efficiency η_r [Fig. 4(d)], this small u-s deviation makes $Mg_{3.2}Sb_{1.5}Bi_{0.49}Te_{0.01}$ as efficient as SnSe or PbTe.

In summary, we investigated the relationship between the microstructure and thermoelectric transport in sintered $Mg_{3.2}Sb_{1.5}Bi_{0.49}Te_{0.01}$ samples. By increasing the grain-size from 1.0 to 7.8 μm, the Hall mobility considerably improved in a broad temperature range, while the thermal conductivity remained intact. The calculated conversion efficiency reaches 14.5%, which is as excellent as other state-of-the-art thermoelectric materials. We also confirmed good thermal stability of $Mg_{3.2}Sb_{1.5}Bi_{0.49}Te_{0.01}$ against an oxidizing atmosphere (supplementary material S4). The high thermoelectric performance in its pristine polycrystalline form is advantageous for practical applications of waste heat recovery.

See supplementary material for the crystal structure refinement, the details of EBSD mapping, the composition analysis, and the thermal stability study.

The NU group was supported by the NASA Science Mission Directorate's Radioisotope Power Systems Thermoelectric Technology Development program. The use of the Advanced Photon Source at Argonne National Laboratory was supported by the U. S. Department of Energy, Office of Science, Office of Basic Energy Sciences, under Contract No. DE-AC02-06CH11357.

[1]L. E. Bell, Science **321**, 1457 (2008).
[2]G. J. Snyder and E. S. Toberer, Nat. Mater. **7**, 105 (2008).
[3]L.-D. Zhao, G. Tan, S. Hao, J. He, Y. Pei, H. Chi, H. Wang, S. Gong, H. Xu, V. P. Dravid, C. Uher, G. J. Snyder, C. Wolverton, and M. G. Kanatzidis, Science **351**, 141 (2016).
[4]H. J. Wu, L.-D. Zhao, F. S. Zheng, D. Wu, Y. L. Pei, X. Tong, M. G. Kanatzidis, and J. Q. He, Nat. Commun. **5**, 4515 (2014).
[5]H. Tamaki, H. K. Sato, and T. Kanno, Adv. Mater. **28**, 10182 (2016).
[6]J. Shuai, J. Mao, S. Song, Q. Zhu, J. Sun, Y. Wang, R. He, J. Zhou, G. Chen, D. J. Singh, and Z. Ren, Energy Environ. Sci. **10**, 799 (2017).
[7]J. Zhang, L. Song, S. H. Pedersen, H. Yin, L. T. Hung, and B. B. Iversen, Nat. Commun. **8**, 13901 (2017).
[8]J. Mao, Y. Wu, S. Song, Q. Zhu, J. Shuai, Z. Liu, Y. Pei, and Z. Ren, ACS Energy Lett. **2**, 2245 (2017).
[9]J. Zhang, L. Song, A. Mamakhel, M. R. V. Jørgensen, and B. B. Iversen, Chem. Mater. **29**, 5371 (2017).
[10]J. Mao, J. Shuai, S. Song, Y. Wu, R. Dally, J. Zhou, Z. Liu, J. Sun, Q. Zhang, C. dela Cruz, S. Wilson, Y. Pei, D. J. Singh, G. Chen, C.-W. Chu, and Z. Ren, PNAS **114**, 10548 (2017).
[11]H. Tamaki, T. Kanno, H. Sato, A. Sakai, and K. Takahashi, Japan patent PCT/JP2016/000811 (27 October 2015).
[12]S. Ohno, K. Imasato, S. Anand, H. Tamaki, S. D. Kang, P. Gorai, H. K. Sato, E. S. Toberer, T. Kanno, and G. J. Snyder, "Phase boundary mapping to obtain *n*-type Mg_3Sb_2-based thermoelectrics," Joule (published online).
[13]F. J. Humphreys, J. Mater. Sci. **36**, 3833 (2001).
[14]A. Togo, L. Chaput, and I. Tanaka, Phys. Rev. B **91**, 094306 (2015).
[15]T. Shiga, J. Shiomi, J. Ma, O. Delaire, T. Radzynski, A. Lusakowski, K. Esfarjani, and G. Chen, Phys. Rev. B **85**, 155203 (2012).
[16]W. Li, L. Lindsay, D. A. Broido, D. A. Stewart, and N. Mingo, Phys. Rev. B **86**, 174307 (2012).
[17]J. Shiomi, K. Esfarjani, and G. Chen, Phys. Rev. B **84**, 104302 (2011).
[18]S. D. Kang and G. J. Snyder, Nat. Mater. **16**, 252 (2017).
[19]B. M. Askerov, *Electron Transport Phenomena in Semiconductors* (World Scientific, 1994).
[20]J. J. Kuo, S. D. Kang, K. Imasato, H. Tamaki, S. Ohno, T. Kanno, and G. J. Snyder, "Grain boundary dominated charge transport in Mg_3Sb_2-based compounds," Energy Environ. Sci. (in press).
[21]G. J. Snyder and T. Ursell, Phys. Rev. Lett. **91**, 148301 (2003); G. J. Snyder, *Thermoelectrics Handbook: Macro to Nano* (CRC, Boca Raton, FL, 2006), Chap. 9.
[22]G. J. Snyder and A. H. Snyder, Energy Environ. Sci. **10**, 2280 (2017).